https://doi.org/10.5194/gchron-2022-24
Preprint. Discussion started: 30 September 2022

GEOCHRONOLOGY Discussions Open Access EGU

DQPB: software for calculating disequilibrium U-Pb ages

Timothy Pollard[1,2], Jon Woodhead[1], John Hellstrom[1], John Engel[1], Roger Powell[1], and Russell Drysdale[1,2]

[1]School of Geography, Earth and Atmospheric Sciences, University of Melbourne, Melbourne, Victoria 3010, Australia
[2]EDYTEM UMR CNRS 5204, Université Savoie Mont Blanc, F-73376 Le Bourget du Lac Cedex, France.

Correspondence: Timothy Pollard (pollard@student.unimelb.edu.au)

Abstract.

DQPB is software for calculating U-Pb ages while accounting for the effects of radioactive disequilibrium among intermediate nuclides of the U-series decay chains. The software is written in Python and distributed both as a pure Python package, and a stand-alone GUI application that integrates with standard Microsoft Excel spreadsheets. The software implements disequilibrium U-Pb equations to compute ages using various approaches, including concordia-intercept ages on a Tera-Wasserburg diagram, disequilibrium U-Pb isochron ages, Pb/U ages based on single analyses, and modified $^{207}\mathrm{Pb}$ ages. These age calculation approaches are tailored toward young materials that cannot reasonably be assumed to have attained radioactive equilibrium at the time of analysis, although they may also be applied to older materials where disequilibrium is no longer analytically resolvable. The software allows users to implement a variety of regression algorithms using both classical and robust statistics approaches, compute weighted average ages, and construct customisable, publication-ready plots of U-Pb age data. Age uncertainties are propagated using Monte Carlo methods.

1 Introduction

With the exception of major uranium-bearing phases, rocks and minerals younger than a few million years were once considered virtually inaccessible to U-Pb methods owing to difficulties inherent in measuring the small quantities of radiogenic-Pb generated over such short time periods (Getty and DePaolo, 1995). However, analytical advances over the past two decades, including improvements in pre-screening (Rasbury and Cole, 2009), sample preparation (e.g., Engel et al., 2020), and mass spectrometry (e.g., Getty and DePaolo, 1995; Woodhead et al., 2006; Sakata et al., 2014), have opened up the possibility of accurately and precisely dating materials as young as Late Pleistocene age. These methodologies are now widely applied to radiogenic-Pb rich minerals including zircon (e.g., Paquette et al., 2019), as well as common-Pb rich materials such as carbonates (e.g., Richards et al., 1998), using both bulk, and laser-ablation/SIMS sampling techniques. In addition to analytical challenges in applying the U-Pb geochronometer to such young materials, another major issue lies in the need to accurately account for the effects of initial radioactive disequilibrium among intermediate nuclides of the U-series decay chains. For older samples the effects of initial disequilibrium are often small relative to the precision of individual age determinations, but in younger materials, failure to correct for these effects can lead to large inaccuracies in final calculated ages (Ludwig, 1977).

https://doi.org/10.5194/gchron-2022-24
Preprint. Discussion started: 30 September 2022

Secondary carbonates, such as speleothems, are well-known to be deposited out of radioactive equilibrium with respect to $^{234}U/^{238}U$, reflecting the $^{234}U/^{238}U$ ratios in the parent waters from which they form (Osmond and Cowart, 1992). Moreover, the insolubility of Th and Pa in these parent waters, leads to their near exclusion from newly precipitated carbonate, causing an additional component of disequilibrium (Richards et al., 1998). On the other hand, igneous minerals formed in high-temperature environments tend to be deposited at, or very close to, radioactive equilibrium with respect to $^{234}U/^{238}U$, but out of equilibrium with respect to Th and Pa (Schoene, 2014). For example, minerals such as zircon tend to exclude Th during crystallisation, while Th-rich phases such as monazite incorporate an initial excess of Th (Schärer, 1984). Over time, any initial excess or deficiency of intermediate nuclides gradually decreases as the U-series decay chains evolve toward radioactive equilibrium, eventually reaching a point after about six half-lives where disequilibrium effects are too small to be measured using current analytical techniques. For carbonates, this is typically ~1.5 Ma for both $^{234}U/^{238}U$ and $^{230}Th/^{238}U$, since evolution of ^{230}Th toward equilibrium is constrained to follow that of the preceding nuclide ^{234}U. For high-temperature minerals formed in equilibrium with respect to $^{234}U/^{238}U$ but out of equilibrium with respect to $^{230}Th/^{238}U$, this age limit is typically closer to ~ 0.5 Ma.

There are two main approaches to accounting for the effects of radioactive disequilibrium on U-Pb ages. The first of these is applicable to samples that can reasonably be assumed to have attained radioactive equilibrium at the time of analysis. This involves correcting Pb*/U isotope ratios (where * denotes radiogenic Pb formed in situ by decay of U) for any excess or deficiency of intermediate nuclides relative to their radioactive equilibrium values (Schärer, 1984). In a closed system, each daughter nuclide in initial excess or deficiency of equilibrium will cause an equivalent over or under abundance of Pb* once radioactive equilibrium is established (Mattinson, 1973). Therefore, it is possible to apply a relatively straightforward correction by adding or subtracting this excess or deficit of Pb*, provided the initial disequilibrium state is known or can be reliably estimated. Ages can then be computed using the regular U-Pb equations that disregard in-growth and decay of intermediate nuclides.

However, for younger samples, which cannot be assumed to be in a state of radioactive equilibrium at the time of analysis, it is necessary to replace the familiar U-Pb age equations with more complete expressions that can account for the growth and decay of intermediate nuclides through time. Equations of this form were first presented for the U-Pb system by Ludwig (1977) based on Bateman's (1910) general solution to differential equations describing time evolution of radionuclides for an arbitrary linear decay chain. Later, Wendt and Carl (1985) presented an alternative version of these equations which includes some simplifications, whilst Guillong et al. (2014) and Sakata et al. (2017) provide equations accounting for disequilibrium in a single intermediate nuclide only. These "disequilibrium U-Pb" equations are general and can also be applied to older samples that have, in a practical sense, attained radioactive equilibrium at the time of analysis. On the other hand, inappropriate use of the Pb* correction approach described above can lead to large over- or under-correction, and thus inaccuracy in calculated ages, over timescales similar to those in which analytically resolvable disequilibrium persists (Fig. 1).

Because these more complete disequilibrium U-Pb equations are rather cumbersome to work with, they are most conveniently implemented using specialised software or in-house computer code. Various approaches have been devised to achieve this. `Isoplot` (Ludwig, 2012) is probably still the most widely used software within the geochronology community and con-

https://doi.org/10.5194/gchron-2022-24
Preprint. Discussion started: 30 September 2022

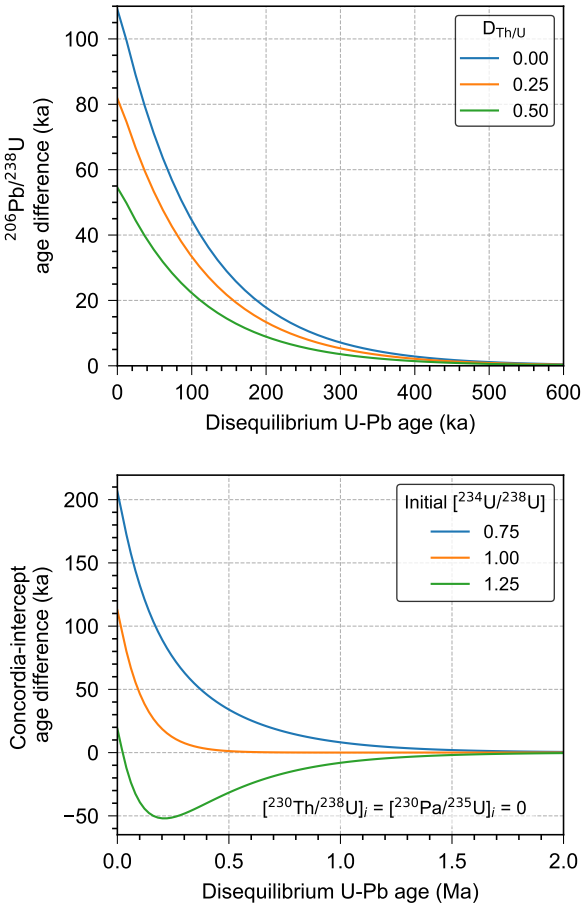

Figure 1. Comparison of U-Pb ages calculated using two different approaches: (i) ages corrected for disequilibrium assuming radioactive equilibrium has been established at the time of analysis, and (ii) ages calculated using the more accurate disequilibrium U-Pb equations which account for growth and decay of intermediate nuclides through time (e.g., Eq. 1 and 7). Age difference is given as age calculated via approach i (assumed equilibrium at time of analysis) minus age calculated via approach ii (more accurate approach). The top panel shows a comparison of zircon $^{206}Pb/^{238}U$ ages calculated assuming various $D_{Th/U}$ (mineral-magma Th/U distribution coefficient) values. The bottom panel shows a comparison of Tera-Wasserburg concordia-intercept ages for carbonate samples with various initial [$^{234}U/^{238}U$] values.

tains in-built functions based on Ludwig (1977) that may be used to calculate disequilibrium U-Pb ages as part of a spreadsheet-based approach. However, this has a number of limitations. Firstly, `Isoplot`, which is distributed as an Excel add-in, is no longer being maintained and is incompatible with recent versions of Excel. Secondly, the `Isoplot` code is protected and hence not readily modified or extended, for example, to produce plots of disequilibrium U-Pb age data. Thirdly, numerical computing and plotting within the Excel environment is relatively limited. More recently, other software packages for handling

https://doi.org/10.5194/gchron-2022-24
Preprint. Discussion started: 30 September 2022

disequilibrium U-Pb age data have been developed (Engel et al., 2019), or are in the developmental stage (additions to the `Isoplot-R` package of Vermeesch, 2018), although these solutions are either not yet documented or difficult to implement as part of a stand-alone workflow for those with little computer programming experience.

Here we introduce `DQPB`, a software package for calculating disequilibrium U-Pb ages. `DQPB` implements the equations of Ludwig (1977) to calculate ages using approaches that are suited to a variety of young sample types. The following sections outline software functionality and discuss approaches implemented for age calculation, error propagation, linear regression, weighted average calculations, and plotting.

2 Software overview

`DQPB` is written in Python, an interpreted, high-level, general-purpose programming language that is rapidly gaining popularity within the geosciences. `DQPB` is available both as a regular Python package and a stand-alone application that does not require users to have a separate Python distribution pre-installed (see Sect. 9 for further details). Python offers several advantages as a language for scientific software development, including its open-source status, well-equipped libraries of functions and routines for scientific computing, and relatively easy-to-read syntax (e.g., Oliphant, 2007). Being a general-purpose language, Python also offers significant advantages in developing stand-alone graphical user interface (GUI) based applications, when compared to "domain specific" scientific languages such as MATLAB and R.

`DQPB` is built on the core Python scientific computing libraries `NumPy` (Harris et al., 2020), `SciPy` (Virtanen et al., 2020) and `Matplotlib` (Hunter, 2007). It also takes advantage of `PyQt` to provide a modern GUI on macOS and Windows, and `xlwings` to facilitate integration with Microsoft Excel. This allows users to select data from an open Excel spreadsheet, perform calculations via the graphical interface, and have results (both numeric and figures) output to the same spreadsheet once computations are complete. In this way, it emulates the ease of use of the popular `Isoplot` program (Ludwig, 2012). As is common practice with open-source software, all Python source code is available for viewing, download, and modification, via an online code repository (see Sect. 9).

3 Disequilibrium U-Pb age calculations

`DQPB` employs an modified version of the equations of Ludwig (1977) to calculate U-Pb ages and plot disequilibrium age data. These equations were initially derived by Ludwig from a form of Bateman's 1910 solution which assumes zero initial abundance of all intermediate daughter nuclides, and independently considers in-growth of Pb* from decay of the primordial parent and each preceding intermediate nuclide (see also Ivanovich and Harmon, 1992; Neymark et al., 2000). These separate components are then summed, or "superposed" (Bateman, 1910), to obtain the total quantity of Pb* as a function of time (t).

Following this approach for the ^{238}U decay chain, and ignoring intermediate nuclides with a half-life less than or equal to that of ^{210}Pb (i.e., $\sim$ 22 a), results in an equation of the form:

$$F = F_1 + F_2 + F_3 + F_4, \quad (1)$$

https://doi.org/10.5194/gchron-2022-24
Preprint. Discussion started: 30 September 2022

where $F = {}^{206}\mathrm{Pb}^*/{}^{238}\mathrm{U}$, and each term represents in-growth from the primordial parent (subscript 1) and each preceding intermediate daughter nuclide in the decay chain (subscripts >1). In full, these individual components are

$$F_1 = e^{\lambda_{238}t}\left(c_1 e^{-\lambda_{238}t} + c_2 e^{-\lambda_{234}t} + c_3 e^{-\lambda_{230}t} + c_4 e^{-\lambda_{226}t} + 1\right) \tag{2}$$

$$F_2 = \frac{\lambda_{238}}{\lambda_{234}}\left[\frac{^{234}\mathrm{U}}{^{238}\mathrm{U}}\right]_{init.} e^{\lambda_{238}t}\left(h_1 e^{-\lambda_{234}t} + h_2 e^{-\lambda_{230}t} + h_3 e^{-\lambda_{226}t} + 1\right) \tag{3}$$

$$F_3 = \frac{\lambda_{238}}{\lambda_{230}}\left[\frac{^{230}\mathrm{Th}}{^{238}\mathrm{U}}\right]_{init.} e^{\lambda_{238}t}\left(p_1 e^{-\lambda_{230}t} + p_2 e^{-\lambda_{226}t} + 1\right) \tag{4}$$

$$F_4 = \frac{\lambda_{238}}{\lambda_{226}}\left[\frac{^{226}\mathrm{Ra}}{^{238}\mathrm{U}}\right]_{init.} e^{\lambda_{238}t}\left(1 - e^{-\lambda_{226}t}\right) \tag{5}$$

where square brackets denote activity ratios, and c, h, and p, are Bateman coefficients given by equation (6) in Ludwig (1977), i.e.,

$$c_i/h_i/p_i = \frac{\prod_{j=1}^{n-1}\lambda_j}{\prod_{j=1}^{n}(\lambda_j - \lambda_i)} \tag{6}$$

where n is the number of nuclides in the portion of the decay chain under consideration (this includes ^{206}Pb, for which $\lambda = 0$, but excludes any preceding nuclides for h and p). Similarly, for the ^{235}U decay chain we have

$$G = G_1 + G_2 \tag{7}$$

where $G = {}^{207}\mathrm{Pb}^*/{}^{235}\mathrm{U}$ and

$$G_1 = e^{\lambda_{235}t}\left(d_1 e^{-\lambda_{235}t} + d_2 e^{-\lambda_{231}t} + 1\right) \tag{8}$$

$$G_2 = \frac{\lambda_{235}}{\lambda_{231}}\left[\frac{^{231}\mathrm{Pa}}{^{235}\mathrm{U}}\right]_{init.} e^{\lambda_{235}t}\left(1 - e^{-\lambda_{231}t}\right) \tag{9}$$

where d is Bateman coefficient defined in an equivalent manner. These equations may alternatively be expressed in a matrix-based form (e.g., Albarède, 1995), which is arguably more mathematically elegant, however, we have opted to preserve the original Ludwig (1977) equations for the purpose of clarity and because we see no practical computational advantage in adopting the matrix approach here. These equations may be employed to compute ages using single-analysis or diagrammatic approaches in a similar fashion to the more familiar U-Pb equations, although they require numerical methods to solve in all instances (see discussion below).

When dealing with materials young enough to retain $\left[^{234}\mathrm{U}/^{238}\mathrm{U}\right]$ or $\left[^{230}\mathrm{Th}/^{238}\mathrm{U}\right]$ values that are analytically resolvable from radioactive equilibrium, it is generally more accurate to use present-day (i.e., measured) activity ratios rather than assumed initial values. This information can be incorporated into the above equations by employing an "inverted" form of the U-series age equations, whereby initial activity ratios are expressed as a function of present-day ratios and t (Woodhead et al., 2006). These equations may then be substituted into the disequilibrium U-Pb equations above and included in the numerical solving procedure, resulting in a solution to both age and the initial activity ratio value. For example, this approach has been widely applied to Quaternary speleothems using measured $\left[^{234}\mathrm{U}/^{238}\mathrm{U}\right]$ values (e.g., Pickering et al., 2011; Bajo et al., 2012).

https://doi.org/10.5194/gchron-2022-24
Preprint. Discussion started: 30 September 2022

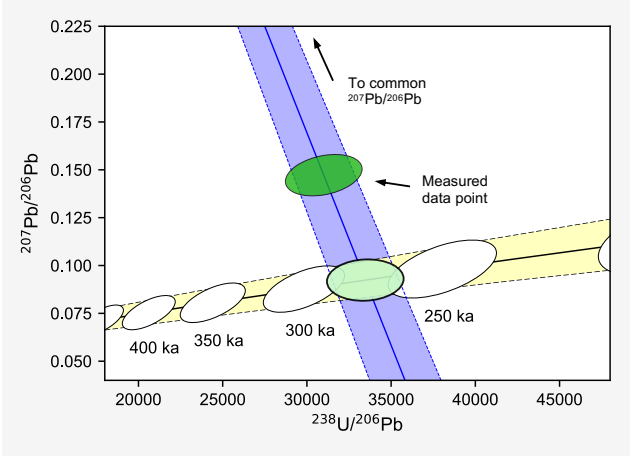

Figure 2. Graphical representation of a modified $^{207}\mathrm{Pb}$ age calculation. A straight line is projected from the $^{207}\mathrm{Pb}/^{206}\mathrm{Pb}_{\mathrm{common}}$ value at the y-axis intercept through measured data points to the disequilibrium concordia curve, constructed here using $\mathrm{D}_{\mathrm{Th/U}}$ = 0.2 ± 0.1 (2σ) and $\mathrm{D}_{\mathrm{Pa/U}}$ = 2.9 ± 0.8 (2σ). Age markers along the disequilibrium concordia are shown as 2σ confidence ellipses (white), which displays uncertainty in x and y arising from assigned distribution coefficient uncertainties (see Sect. 7). The modified $^{207}\mathrm{Pb}$ age of 275 ± 23 ka (2σ) is represented by the pale green ellipse. Note that the equilibrium concordia, if plotted, would appear as a horizontal line along the bottom of this figure at $y \approx 0.046$.

3.1 Pb/U ages based on single analyses

The most straightforward implementation of the disequilibrium U-Pb age equations involves treating each U decay series independently to compute a single-analysis $^{206}\mathrm{Pb}/^{238}\mathrm{U}$ or $^{207}\mathrm{Pb}/^{235}\mathrm{U}$ age. This is achieved by solving

$$F - \left(\frac{^{206}\mathrm{Pb}}{^{238}\mathrm{U}}\right)_{\mathrm{meas.}} = 0 \tag{10}$$

or,

$$G - \left(\frac{^{207}\mathrm{Pb}}{^{235}\mathrm{U}}\right)_{\mathrm{meas.}} = 0 \tag{11}$$

where subscript "meas." denotes a measured Pb/U ratio corrected for blank and common Pb. These age calculations may be applied, for example, in computing $^{206}\mathrm{Pb}/^{238}\mathrm{U}$ ages for young, radiogenic-Pb rich minerals such as Quaternary zircons, provided common Pb is negligible or can be accurately corrected for – e.g., in CA-TIMS studies (von Quadt et al., 2014).

In the more general case where common Pb is not negligible nor amenable to accurate correction based on measurement of $^{204}\mathrm{Pb}$-based ratios (e.g., in samples analysed by ICP-MS techniques), the "modified $^{207}\mathrm{Pb}$" approach proposed by Sakata (2018), is more practically useful. This approach, which is similar to the "single-aliquot" method of Woodhead et al. (2012) for dating of high U/Pb speleothems, involves plotting each data point, uncorrected for common-Pb and disequilibrium on a Tera-Wasserburg diagram ($^{207}\mathrm{Pb}/^{206}\mathrm{Pb}$ vs. $^{238}\mathrm{U}/^{206}\mathrm{Pb}$; Tera and Wasserburg, 1972), and projecting a line from a single common $^{207}\mathrm{Pb}/^{206}\mathrm{Pb}$ value on the y-axis intercept, through each data point to the disequilibrium concordia (Fig. 2). An

https://doi.org/10.5194/gchron-2022-24
Preprint. Discussion started: 30 September 2022

intercept age may then be computed for each data point, assuming concordance between the ^{238}U and ^{235}U decay schemes. This provides a means of correcting ages for common-Pb and disequilibrium in an internally consistent fashion, however, unlike the disequilibrium concordia-intercept approach outlined below (Sect. 3.3), the common Pb composition is not given by linear regression of the data points themselves and must be specified independently. For igneous minerals, this may be achieved using whole rock measurements, analysis of Pb isotope ratios in co-genetic Pb-rich phases (e.g., K-feldspars), or model estimates of average crustal Pb composition such as Stacey and Kramers (1975).

To compute disequilibrium U-Pb ages using these single analysis approaches, it is necessary to specify the initial radioactive disequilibrium state of long-lived intermediate nuclides. For minerals that crystallised from a melt in radioactive equilibrium, initial $[^{230}Th/^{238}U]$ and $[^{231}Pa/^{235}U]$ may be computed based on mineral-melt Th/U and Pa/U distribution coefficients (e.g., McLean et al., 2011) and these values can be substituted into the disequilibrium U-Pb equations above. Two different approaches are typically used to estimate the ratio of Th/U distribution coefficients (i.e., $D_{Th/U}$) for a suite of co-genetic and coeval zircons (e.g., Rioux et al., 2012). The first assumes that Th/U elemental ratio of the melt is constant, but varies across different coeval mineral grains. Using this approach, $Th/U_{min.}$ values (where subscript min. denotes mineral) may be calculated based on direct measurement of $^{232}Th/^{238}U$, under the assumption that ^{232}Th has produced negligible radiogenic ^{208}Pb since the time of system closure (Ito et al., 2017). $D_{Th/U}$ for each mineral grain is then calculated as

$$D_{Th/U} = \frac{(Th/U)_{min.}}{(Th/U)_{melt}} \tag{12}$$

where $(Th/U)_{melt}$ is estimated from whole rock measurements (Schärer, 1984), or measured Th/U in co-genetic volcanic glasses believed to be representative of the original melt composition (e.g., Rioux et al., 2012). The second approach assumes that $D_{Th/U}$ is constant for all mineral grains and thus Th/U of the magma varies. In this case, $D_{Th/U}$ values are typically estimated based on experimental values or average values from geologically similar contexts (e.g., Sakata, 2018). For estimating $D_{Pa/U}$ values, the second approach is more widely applicable owing to difficulties in constraining Pa/U values of the melt, and more easily justified owing to the lower sensitivity of modified ^{207}Pb ages to this value (Sakata et al., 2017).

For multiple co-genetic zircon $^{206}Pb/^{238}U$ ages that are believed to comprise a single statistical population, a weighted average age may be computed using an equivalent approach to conventional Pb/U ages. However, in the case of disequilibrium ages, uncertainty in Th/U_{melt} for the first disequilibrium correction approach outlined above, or $D_{Th/U}$ and $D_{Pa/U}$ for the second, acts as a systemic component of error, giving rise to correlated age uncertainties. These correlations can be non-trivial and should be considered in any weighted average calculation, or alternatively propagated by quadratic addition after taking the weighted average (second approach only) - see Ickert et al. (2015). `DQPB` allows users to compute disequilibrium $^{206}Pb/^{238}U$, $^{207}Pb/^{235}U$ and modified ^{207}Pb ages, specifying the initial disequilibrium state either as a constant $D_{Th/U}$ ($D_{Pa/U}$) value and uncertainty, or an individual $Th/U_{min.}$ ($Pa/U_{min.}$) for each analysis along with a single Th/U_{melt} (Pa/U_{melt}) value. Age uncertainties and uncertainty covariances are estimated by Monte Carlo methods, and where appropriate, weighted average ages accounting for this covariance structure may be computed using either classical or robust statistics approaches (see Sect. 5 for further details).

https://doi.org/10.5194/gchron-2022-24
Preprint. Discussion started: 30 September 2022

3.2 "Classical" U-Pb isochron ages

Disequilibrium ^{238}U-^{206}Pb and ^{235}U-^{207}Pb "classical" isochron ages may be computed for common-Pb rich samples by numerically solving $F - b = 0$, or $G - b = 0$, where b is the slope of the isochron regression line on a $^{206}\mathrm{Pb}/^{204}\mathrm{Pb}$ vs. $^{238}\mathrm{U}/^{204}\mathrm{Pb}$ or $^{207}\mathrm{Pb}/^{204}\mathrm{Pb}$ vs. $^{235}\mathrm{U}/^{204}\mathrm{Pb}$ diagram respectively. For "classical" U-Pb isochron diagrams, isotope ratios are traditionally referenced to $^{204}\mathrm{Pb}$, however, when dating young materials with very low $^{232}\mathrm{Th}$ abundance, such as carbonates with low detrital content, it is also possible to reference to $^{208}\mathrm{Pb}$ under the assumption that $^{232}\mathrm{Th}$ has produced negligible radiogenic $^{208}\mathrm{Pb}$ since the time of system closure (Getty et al., 2001). The two formulations are mathematically equivalent, but the latter can be advantageous where accurate measurement of $^{204}\mathrm{Pb}$ proves difficult, such as in ICP-MS dating of young samples (Engel et al., 2019). While U-Pb isochron approaches can be less reliable than concordia-intercept ages, especially for young data sets incorporating the low abundance $^{204}\mathrm{Pb}$ isotope, they are offered in `DQPB` because of their potential utility in computing ages for Pb-rich materials where the disequilibrium state of only one of the U-series decay chains is well constrained.

3.3 Concordia-intercept ages

Concordia-intercept ages are well-suited to Pb-rich materials such as carbonates and apatite that typically contain variable Pb*/common-Pb ratios within individual growth horizons (Woodhead and Pickering, 2012; Engel and Pickering, 2022; Chew et al., 2011). To compute ages using this approach, multiple co-genetic samples uncorrected for common Pb are plotted on a Tera-Wasserburg diagram. If all samples (i) have remained closed to exchange of U-series isotopes post crystallisation, and (ii) contain varying quantities of common Pb with an identical $^{207}\mathrm{Pb}/^{206}\mathrm{Pb}$ composition, and (iii) were initially crystallised in the same disequilibrium state, they form a mixing line on a Tera-Wasserburg diagram between a purely radiogenic end-member lying on the concordia curve (the locus of all radiogenic Pbs through time) and a common Pb end-member at the y-axis intercept (Tera and Wasserburg, 1972). When accounting for the effects of radioactive disequilibrium, the familiar equilibrium concordia is replaced with a family of disequilibrium concordia constructs (e.g., Wendt and Carl, 1985), based on equations

$$x = \frac{^{238}\mathrm{U}}{^{206}\mathrm{Pb}^*} = \frac{1}{F} \tag{13}$$

and,

$$y = \frac{^{207}\mathrm{Pb}^*}{^{206}\mathrm{Pb}^*} = U^{-1}Gx \tag{14}$$

where U denotes the present-day natural $^{238}\mathrm{U}/^{235}\mathrm{U}$ ratio. Activity ratios may either be input directly into functions F and G as initial values, or as present-day values via the inverted U-series equations as described in Sect. 3, and ages are then calculated as the intersection of regression line with the appropriate concordia curve, by solving

$$U^{-1}G - aF - b = 0 \tag{15}$$

where a and b are the slope and y-intercept values obtained by linear regression of the data points. `DQPB` allows users to fit a variety of regression models to Tera-Wasserburg data (Sect. 4), compute ages based on either initial or present-day intermediate nuclide activity ratios values, and construct customisable plots of the disequilibrium concordia intercept ages (e.g., Fig. 3).

https://doi.org/10.5194/gchron-2022-24
Preprint. Discussion started: 30 September 2022

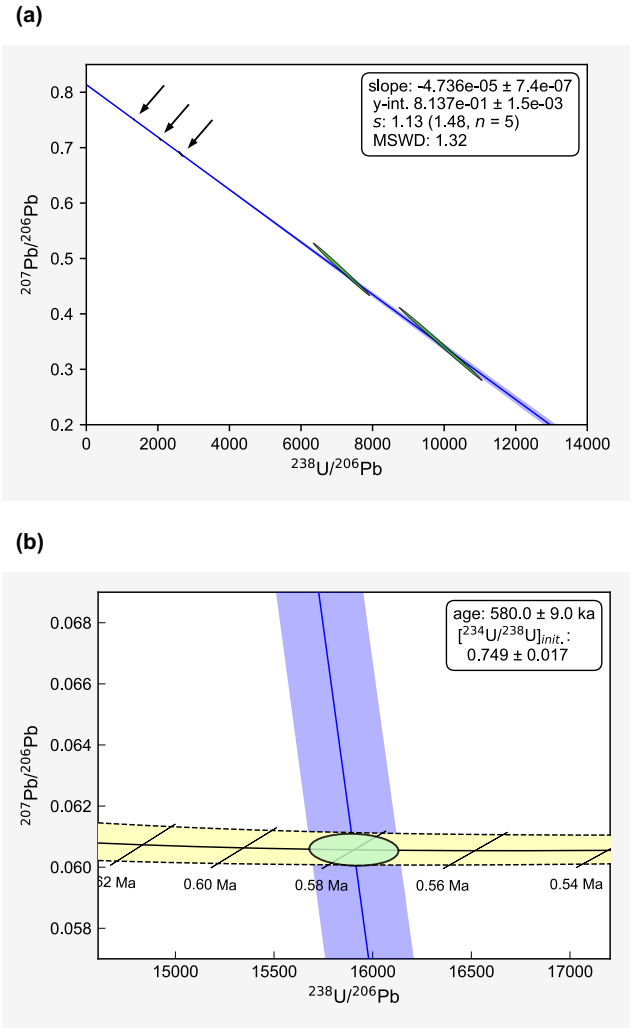

Figure 3. Example concordia-intercept age plots for Mid-Pleistocene stalagmite CCB (see Sect. 8.1 for further details). (a) Tera-Wasserburg plot showing the `spine` linear regression fit to data . Measured data points are represented as 95% confidence region ellipses and exhibit a strong negative error correlation due the effects of blank subtraction (Woodhead et al., 2012). The shaded blue band indicates a 95% confidence limit of the regression fit. (b) Enlarged view of the concordia intercept. The disequilibrium concordia line (black) is based on a measured $[^{234}U/^{238}U]$ value of 0.9512 ± 0.0013 (1σ), with initial activity ratios for other intermediate nuclides assumed equal to 0. The yellow band about the concordia curve shows 2σ uncertainties arising due to uncertainty in this measured $[^{234}U/^{238}U]$ value. The black diagonal lines represent 2σ age "ellipses", which are collapsed to straight line segments because there is no uncertainty assigned to $[^{231}Pa/^{235}U]$ (see Sect. 7). A confidence ellipse representing concordia intercept points for the 50,000 Monte Carlo iterations is shown in pale green.

https://doi.org/10.5194/gchron-2022-24
Preprint. Discussion started: 30 September 2022

3.4 Forced-concordance initial $\left[^{234}\mathrm{U}/^{238}\mathrm{U}\right]$ values

DQPB also implements a version of the "forced concordance" routine of Engel et al. (2019), which targets closed-system samples where the initial $^{234}\mathrm{U}/^{238}\mathrm{U}$ activity ratio is unknown, but activity ratios of other long-lived intermediate nuclides (i.e., $[^{230}\mathrm{Th}/^{238}\mathrm{U}]$ and $[^{231}\mathrm{Pa}/^{235}\mathrm{U}]$) are reliably constrained (e.g., very low initial Th carbonates). The routine determines the $\left[^{234}\mathrm{U}/^{238}\mathrm{U}\right]$ value that forces concordance between the $^{235}\mathrm{U}$–$^{207}\mathrm{Pb}$ and $^{238}\mathrm{U}$–$^{206}\mathrm{Pb}$ decay schemes, and outputs this value along with its uncertainty computed by Monte Carlo methods. This algorithm may be useful for characterising initial $\left[^{234}\mathrm{U}/^{238}\mathrm{U}\right]$ values for particular geological contexts (e.g., cave sites when dating carbonate speleothems) where all available samples lie beyond the range of measurable disequilibrium.

4 Regression protocols

Linear regression algorithms capable of accounting for analytical uncertainties and accommodating the possibility of "excess scatter" (i.e., scatter in excess of that due to assigned analytical uncertainties) are crucial to attaining reliable U-Pb isochron and concordia-intercept ages. DQPB offers two different approaches to regression fitting. The first is rooted in a classical statistics paradigm and emulates the default regression fitting protocols of Isoplot (Ludwig, 2012). The second approach takes advantage of recent developments in the application of robust statistics to isochron fitting, implementing the spine algorithm of Powell et al., (2020), as well as a newly developed robust regression algorithm.

For the classical statistics-based approach, linear regression of the data is first performed using the error-weighted least-squares algorithm of York et al. (2004) (which gives equivalent results to the original algorithm of York (1969) with analytical uncertainties calculated following the Maximum-Likelihood Estimation approach of Titterington and Halliday (1979)). An apparent advantage of this algorithm is that it allows a statistic with a well-established established distribution, the mswd (mean square of weighted deviates), to be used to assess data point scatter in relation to measurement uncertainties, under the assumption that residuals are strictly Gaussian distributed (Wendt and Carl, 1991). Probabilistic-based conclusions can then be drawn regarding the likely presence (or not) of excess scatter.

Where mswd lies within a probabilistically acceptable range, as indicated either by a confidence interval on mswd (e.g., Powell et al., 2002), or equivalently, the "probability-of-fit" value (Ludwig, 2012), the initial York fit and analytical uncertainties are retained. However, if the mswd value falls outside such limits, the dataset is deemed likely to contain a component of excess scatter, which may be either "geological scatter" (variability in initial Pb composition, open-system behaviour etc.) or some unaccounted-for component of analytical uncertainty. Provided the mswd is not unreasonably high, analytical uncertainties likely still dominate the uncertainty budget, and, on this basis, the York fit parameters are retained but data point uncertainties are expanded so as to reduce the re-computed mswd to 1 (i.e., the "model 1x" borrowing the terminology of Powell et al., 2020). On the other hand, where mswd lies well outside a probabilistically acceptable range, the assumptions of the York fit are clearly violated, and it is commonplace to turn to other classical statistics based approaches, for example, by employing the Isoplot model 2 or model 3 fits (Ludwig, 2012).

https://doi.org/10.5194/gchron-2022-24
Preprint. Discussion started: 30 September 2022

Although this classical-statistics approach to regression fitting is widely adopted within geochronology, it has some limitations. Firstly, it relies on a stepwise approach to error handling, which is both conceptually unsatisfying and requires choice of arbitrary cut-off points, the values of which can have a substantial impact on calculated ages and uncertainties (see Powell et al., 2020). Secondly, `mswd` is very sensitive to small departures in residuals from a strict Gaussian distribution, making it an overly sensitive indicator of excess scatter for many real-world geochronological data sets, which are often slightly "fat tailed" (Powell et al., 2002). Thirdly, the model 2 and 3 algorithms are not well-suited to all data sets. For example, the model 3 fit parameterises excess scatter as an external Gaussian-distributed component or variance, an assumption which is difficult to justify in the typical case where the precise cause of excess scatter is not well-established nor known to be strictly Gaussian (Ludwig, 2003). The model 2 fit, on the other hand, makes few assumptions regarding the statistical distribution of the excess scatter, however, it weights all data points equally and does not account for analytical uncertainties at all.

In an effort to address these limitations, `DQPB` implements the robust `spine` algorithm of Powell et al. (2020) as the default regression fitting algorithm for all data sets. The `spine` algorithm exhibits a number of favourable properties that arguably make it more generally applicable to U-Pb datasets compared to the classical statistics approach outlined above, and improves on previous robust approaches to isochron fitting (e.g., Rock and Duffy, 1986) by accounting for assigned analytical uncertainties.

The `spine` algorithm minimises a piece-wise objective function (the "Huber loss function"), whereby data points lying along a central linear band (i.e., the "spine") are given full weighting, but points falling outside this band are progressively down-weighted according to their weighted residual. Uncertainties on regression parameters are then calculated using a first-order error propagation approach and tend to increase smoothly with increasing data point scatter. Notably, in the special case where all data points lie within this central band, `spine` yields identical results to `York`, making this algorithm suitable for both "well-behaved" and excess scatter data sets, provided that the majority of data points comprise a well-defined linear array within their uncertainties.

In place of the `mswd`, a robust metric called the spine width, s, is used to assess whether or not data point scatter is consistent with the minimal assumptions of this algorithm. s is the median absolute deviation (`nmad`) of weighted residuals, normalised to be equal to the standard deviation for a strictly Gaussian distribution. This statistic tends toward 1 for well-behaved data sets and may be employed in a similar fashion to the `mswd`, although, in contrast to `mswd`, confidence limits on spine width must be derived from simulation rather than from a formal statistical distribution (Powell et al., 2020). `DQPB` outputs s along with this simulated upper 95% confidence bound, allowing users to assess if the central spine of data is sufficiently well-defined for accurate use of this algorithm.

A second robust regression approach is also offered for datasets that have an s value exceeding this upper confidence limit, but are still believed to contain age significance (see Appendix C). This regression algorithm, termed the "Robust model 2", is similar to the `Isoplot` model 2, but encompasses robust properties which reduce the influence of outliers on the fitted line in a similar manner to `spine`. Although this algorithm discards analytical uncertainties and provides less reliable age uncertainty estimates than `spine`, it is offered as a robust alternative to the model 2 and 3 fits discussed above, as it should be suitable for a wider range of data sets.

https://doi.org/10.5194/gchron-2022-24
Preprint. Discussion started: 30 September 2022

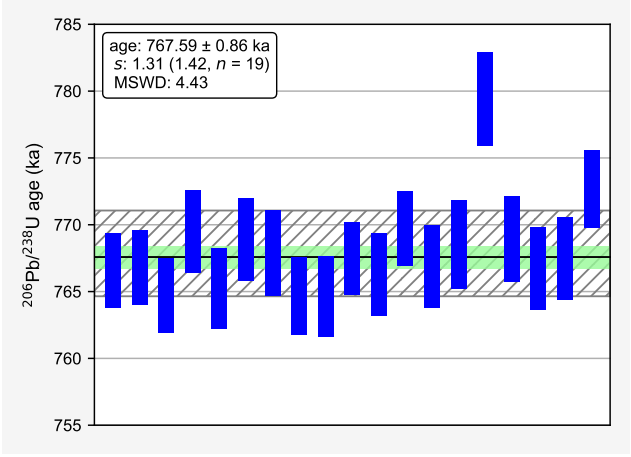

Figure 4. A comparison of the `spine` weighted average age with the classical statistics weighted mean for Bishop Tuff zircon $^{206}\mathrm{Pb}/^{238}\mathrm{U}$ ages from Crowley et al. (2007). The black line shows the `spine` weighted average $^{206}\mathrm{Pb}/^{238}\mathrm{U}$ age of 767.59 ± 0.86 ka, with 2σ uncertainties (excluding decay constant uncertainties) given by the light green shading. The s value for this data set is 1.31, which is comfortably within the upper 95% confidence limit value on s (1.42, $n = 19$), suggesting the data set contains a sufficiently well-defined "spine" of single-analysis ages for use of this algorithm. For comparison, the classical statistics weighted mean age is 767.85 ± 1.5 ka (`mswd` = 4.43, n = 19), with the 2σ uncertainty envelope represented by the grey hatched area. If the two oldest ages are treated as outliers (as for the preferred age in the original publication) the classical weighted mean shifts to 767.06 ± 0.85 ka (`mswd`=1.3, n=17). Note that age uncertainty covariances have not been considered in this example, although the `spine` algorithm is capable of accounting for these (see Sect. 5).

5 Weighted average age calculations

When dealing with multiple ages that are believed to comprise a single statistical population, e.g., $^{206}\mathrm{Pb}/^{238}\mathrm{U}$ ages from multiple co-genetic and coeval zircon grains, it is commonplace to compute a weighted average age under the assumption that scatter in the individual ages arises from analytical uncertainty alone. This is typically achieved by weighting individual ages according to the inverse of their analytical variance, possibly accounting for the uncertainty covariance structure (e.g., McLean et al., 2011). As in the classical statistics approach to regression fitting, the `mswd` value is then used to assess whether age scatter is commensurate with analytical uncertainties, based on the "probability of fit" value or confidence limits on `mswd`. Where the `mswd` value clearly lies outside a probabilistically acceptable range, but the data are still believed to constitute a single geologically meaningful age population, it is commonplace to either manually reject one or more "outliers" and recompute the weighted mean, or alternatively parameterise this additional scatter as an external Gaussian-distributed component of uncertainty (e.g., Ludwig, 2012).

Because this approach is subject to many of the same limitations as the classical statistics-based regression fitting approach outlined above, `DQPB` offers an alternative algorithm for computing weighted average ages based on robust statistics. Robust statistics approaches of varying complexity have previously been adopted in geochronology, ranging from use of the simple median along with confidence intervals based on the Wilcoxon signed-rank test (Rock et al., 1987) to Tukey's Biweight mean

https://doi.org/10.5194/gchron-2022-24
Preprint. Discussion started: 30 September 2022

(Ludwig, 2012). However, a limitation of these approaches is that they ignore analytical uncertainties, leading to suboptimal results where these analytical uncertainties do in fact constitute a significant component of the total data point scatter. In place of these algorithms, `DQPB` offers an algorithm for computing weighted averages that is based on a 1-dimensional version of the `spine` algorithm and is capable of accounting for assigned analytical uncertainties and uncertainty correlations (see Appendix A). Like the `spine` regression algorithm, the `spine` weighted average gives full analytical weighting to ages at the centre of the distribution, and progressively down-weights those lying away from this central 'spine' according to the Huber loss function. In the case where data point scatter is commensurate with analytical uncertainties, the `spine` weighted average reduces to the classical statistics weighted mean (e.g., Powell and Holland, 1988; McLean et al., 2011). As for the `spine` regression algorithm, the quality of this central 'spine' of data points can be assessed by considering the spine width in relation to its upper 95% confidence bound, derived via simulation of Gaussian distributed data sets (see Appendix B). `DQPB` outputs this information along with weighted average age results (see Fig. 4 and 5b).

6 Error propagation

`DQPB` employs Monte Carlo methods to estimate uncertainties for all age types. For concordia-intercept and "classical" isochron datasets fitted either using robust or model 1 algorithms, regression parameters are randomised within uncertainties according to a bivariate Gaussian distribution for each iteration, accounting for uncertainty correlation between the slope and y-intercept. For model 1x, model 2 and model 3 fits, (i.e., "excess scatter" fits) regression parameters are instead randomised within their "observed scatter" uncertainties, i.e., 1σ internal errors multiplied by $\sqrt{\texttt{mswd}}$ according to a bivariate t distribution with $n-2$ degrees of freedom, n being the number of data points. Activity ratios, either as initial or present-day values, are then randomised according to univariate Gaussian distribution, and an age is computed for each combination of inputs. Where a present-day activity ratio value is given, the initial activity ratio value is also computed for each iteration as part of the numerical solving procedure. Age uncertainties are reported as a 95% confidence interval, estimated from the 2.5 and 97.5 percentiles of simulated ages. In most cases these upper and lower bounds are symmetric and Gaussian distributed, although this is not necessarily the case for concordia-intercept ages with large regression parameter uncertainties.

For single-analysis Pb/U ages, isotope ratios for each data point are first randomised within their uncertainties according to a univariate Gaussian distribution, or a multivariate Gaussian distribution for modified $^{207}\mathrm{Pb}$ ages. Variables that contribute a systematic component of uncertainty, such as distribution coefficient, $\mathrm{Th/U_{melt}}$ values (and common $^{207}\mathrm{Pb}/^{206}\mathrm{Pb}$ values for modified $^{207}\mathrm{Pb}$ ages) are randomised within their uncertainties once per iteration, and these simulated values are used to compute an age for each data point. This results in an m-by-n array where n is the number of single-analysis ages and m is the number of Monte Carlo trials. Age uncertainties on individual analysis are reported as a 95% confidence interval and age covariances are estimated from simulated ages for each of the n data points, resulting in an n-by-n covariance matrix. Where appropriate, this estimated covariance structure is then be employed in subsequent weighted average age calculations.

`DQPB` offers options to reject iterations that return negative ages and/or initial activity ratio solutions (if present-day activity ratio values are used), and iterations where negative activity ratios are simulated during the initial randomisation stage. Full

https://doi.org/10.5194/gchron-2022-24
Preprint. Discussion started: 30 September 2022

details on the number of rejected iterations and the reason for rejection are provided to the user, and histograms and scatterplots of all simulated Monte Carlo values can also be optionally output to visually scrutinise results. Decay constant uncertainties, and uncertainties in present-day $^{238}U/^{235}U$ values for disequilibrium concordia-intercept and modified ^{207}Pb ages, may also be included in Monte Carlo simulations, and are treated as systemic sources of uncertainty where relevant, although the effects of these sources of uncertainty are negligible over timescales most relevant to disequilibrium U-Pb dating.

7 Data visualisation and plotting

DQPB outputs highly customisable plots for all diagrammatic and weighted average U-Pb age calculations. For isochron ages, a plot showing data points as 95% confidence ellipses is provided, along with the regression line. An error envelope about the regression line, indicating a 95% confidence band on the regression fit may also be plotted using the approach of Ludwig (1980) for model 1–3 fits, or Monte Carlo simulation for robust fits (e.g. Fig. 3a). For concordia intercept ages, an additional plot is output showing an enlarged view of the intersection between the isochron and the disequilibrium concordia curve (e.g. Fig. 3b). The intercept points of all Monte Carlo simulated ages are also shown on this plot, either as individual x-y points, or plotted as a single 95% confidence ellipse . For modified ^{207}Pb ages, data points are plotted on a Tera-Wasserburg diagram, along with the disequilibrium concordia curve, if $D_{Th/U}$ and $D_{Pa/U}$ are input as constant values for all data points. The projection lines from the common Pb point through each data point to its intercept with the concordia may also be displayed (e.g. Fig. 5a).

For disequilibrium concordia curves on concordia-intercept plots, age markers may either be plotted as regular data point markers, or as "age ellipses" that represent uncertainty in x-y for a given t value arising from uncertainty in activity ratio values. Where there is uncertainty in activity ratios for both the ^{238}U and ^{235}U decay series, these "age ellipse" markers are true ellipses, akin to those representing decay constant uncertainties on an equilibrium Tera-Wasserburg concordia diagram (Ludwig, 1998). On the other hand, where there is activity ratio uncertainty assigned to only one of the decay schemes, these age ellipses collapse to line segments with a slope equivalent to the Tera-Wasserburg "isochron" lines described in Eq. 7 of Wendt and Carl (1985). A 95% confidence band representing uncertainty in the trajectory of the concordia curve due to uncertainty in activity ratios may also be plotted based on Monte Carlo simulation.

DQPB allows users to customise a wide range of plot settings, export figures in a variety of image file formats, and access all numeric data used to construct plots via an Excel spreadsheet (see Supplementary Information for further details).

8 DQPB usage examples

8.1 Concordia-intercept speleothem age

Despite their relatively low U content, clean (i.e., with low detrital content) carbonates, such as speleothems, can be well-suited to U-Pb dating provided they contain relatively high U/Pb ratios and spread in Pb*/common-Pb ratios within individual growth layers (Woodhead et al., 2012). Here we demonstrate computation of a concordia-intercept age for a Middle Pleistocene speleothem CCB from Corchia Cave, Italy, based on solution MC-ICP-MS analyses. The sample is young enough to retain a

https://doi.org/10.5194/gchron-2022-24
Preprint. Discussion started: 30 September 2022

$\left[^{234}U/^{238}U\right]$ ratio which is analytically resolvable from equilibrium but lies just beyond reach of the ^{230}Th geochronometer using routine methods. A measured $^{234}U/^{238}U$ activity ratio of 0.9512 ± 0.0013 (1σ) was used in the age calculation, obtained via MC-ICP-MS (Hellstrom, 2003). Speleothems from this cave site consistently exhibit very low detrital-Th (as reflected in $^{232}Th/^{230}Th$ ratios; Drysdale et al., 2012) and thus the initial $\left[^{230}Th/^{238}U\right]$ is assumed equal to zero. The initial activity ratios for other intermediate nuclides are likewise assumed equal to zero. The data are regressed using the `spine` algorithm, which in this case returns equivalent results to the `York` algorithm (Fig. 3a). A lower intercept age of 580 (571, 589) ka (95% CI) is computed, along with an initial $\left[^{234}U/^{238}U\right]$ value of 0.749 (0.731, 0.766) (95% CI). Age uncertainties are estimated by Monte Carlo simulation using 50,000 trials (Fig. 3b).

8.2 Modified ^{207}Pb Quaternary zircon ages

In this example, we demonstrate a modified ^{207}Pb age calculation for a suite of zircons were separated from the Sambe-Kisuki tephra (Shuhei Sakata, unpublished data), which is believed to have erupted approximately 100 ka ago from the Sambe volcano located in Shimane prefecture in the west of Japan. Analyses were performed by multi-collector LA-ICPMS using a method similar to Hattori et al. (2017). Disequilibrium ages were calculated using an estimated $D_{Th/U}$ value of 0.2 ± 0.03 (2σ), an estimated $D_{Pa/U}$ value of 2.9 ± 1 (2σ), and a common $^{207}Pb/^{206}Pb$ value based on the two-stage model of Stacey and Kramers (1975). Age uncertainties were calculated by Monte Carlo simulation, using 50,000 trials for each age point (Fig. 5a). Computing a weighted average using a classical statistics approach (accounting for uncertainty correlations), gives a weighted mean age of 96.6 ± 39 ka (95% CI), with a `mswd` of 3.54, indicating a very high probability of excess scatter in the dataset under the assumption of Gaussian distributed residuals. On the other hand, the robust `spine` weighted average algorithm gives a weighted average age of 94.2 ± 10.9 ka (95% CI) (Fig. 5b), with a spine width value of 1.28 which lies within the upper 95% confidence limit of s (1.57, n = 6). This suggests that the dataset contains a well-resolved central spine of data, and thus the weighted average is likely to carry age significance under the assumption that crystallisation of these zircons constitutes a geologically discrete event (e.g., see Ickert et al., 2015). Note, the `spine` weighted average algorithm down-weights the single point lying away from the average age line, and thus it has little influence on the computed weighted average. For comparison, excluding this point gives a classical weighted average age of 92.1 ± 6.3 ka (95% CI) with a `mswd` of 0.55.

9 Availability and distribution

`DQPB` is released under a MIT license, permitting modification of the source code and re-distribution with minimal restrictions. The source code may be viewed via an online code repository (see: https://github.com/timpol/DQPB). This repository also contains links to downloadable installers for macOS and Windows and online documentation. Suggestions for bug fixes and new features, as well as pull requests, are also accepted via this repository.

In addition to the stand-alone GUI version of the software, `DQPB` is also available as part of a pure Python package named `pysoplot`, offering greater flexibility for more experienced Python users. The `pysoplot` package is hosted at a separate

https://doi.org/10.5194/gchron-2022-24
Preprint. Discussion started: 30 September 2022

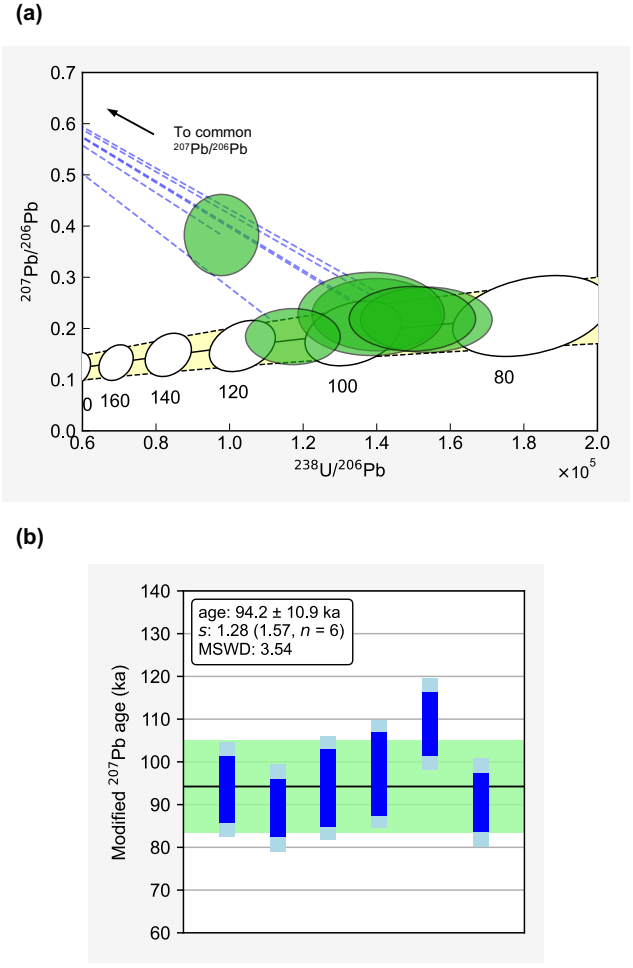

Figure 5. Example modified $^{207}\mathrm{Pb}$ age plots. (a) Data ellipses plotted on a Tera-Wasserburg diagram. The yellow band shows the disequilibrium concordia for $\mathrm{D_{Th/U}} = 0.2$ and $\mathrm{D_{Pa/U}} = 2.9$. The dashed blue lines show a line projecting from the common Pb point at the y-intercept ($^{207}\mathrm{Pb}/^{206}\mathrm{Pb} = 0.836$) through the centre of each data point to its intercept with the disequilibrium concordia. (b) Plot of individual modified $^{207}\mathrm{Pb}$ ages. The dark blue bars indicate 2σ age uncertainties accounting for random analytical uncertainties only, while the light blue bars show 2σ age uncertainties including random and systematic components of uncertiainty (i.e., including age uncertainty due to uncertainty in $\mathrm{D_{Th/U}}$ and $\mathrm{D_{Pa/U}}$ values). The black line shows the weighted average age computed using the robust `spine` algorithm which accounts for the age covariance structure, and the light green shading indicates the 95% confidence interval on this weighted average.

online repository (see: https://github.com/timpol/pysoplot) and is available via pip (the package installer for Python) – see:
385 https://pypi.org/project/pysoplot/.

https://doi.org/10.5194/gchron-2022-24
Preprint. Discussion started: 30 September 2022

10 Conclusion

This paper introduces DQPB, an open-source software package for calculating disequilibrium U-Pb ages. The software implements the equations of Ludwig (1977) to compute ages using various approaches, including disequilibrium single-analysis Pb/U ages, U-Pb isochron ages, and concordia-intercept ages on a Tera-Wasserburg diagram. Various linear regression and weighted average age algorithms are implemented in the software, including those based on both classical and robust statistics. Age uncertainties are computed using Monte Carlo routines, and high quality "publication ready" figures are output. A key feature of the stand-alone GUI based version of the software, is that it allows close integration with Microsoft Excel and thus continues the legacy of Isoplot in allowing straightforward interaction with U-Pb datasets from within a simple spreadsheet environment. DQPB is free open-source software, and all source-code is available for viewing and download via an online repository. For more experiences Python users, DQPB is available as part of a pure Python package, and source code may also be downloaded and modified with minimal restrictions to meet individual requirements. DQPB will continue to be developed under this open-source model and new features will be added in the future.

Appendix A: `spine` robust weighted average

Following the logic of Powell et al. (2020) for the 2-dimensional case, a robust spine weighted average accounting for analytical uncertainties may be obtained for 1-dimensional data (e.g., multiple coeval ages). To achieve this in the general case where correlated age uncertainties are permitted, it is first necessary to express weighted residuals in an uncorrelated form. In the classical statistics solution (e.g., Powell et al., 1988, McLean et al., 2011), the weighted average age is obtained by finding $\bar{t}$, that minimises the sum of squared weighted residuals:

$$S = (\boldsymbol{t} - \bar{t}\mathbf{1})\,{\mathbf{V}_t}^{-1}\,(\boldsymbol{t} - \bar{t}\mathbf{1}) \tag{A1}$$

where $\boldsymbol{t}$ is a column vector of ages, $\mathbf{1}$ is a column vector of ones, and $\mathbf{V}_t$ is the covariance matrix of the ages. To apply the Huber loss function, which is defined as

$$\rho(r_k) = \begin{cases} {r_k}^2 & \text{if } |r_k| \leq h \\ 2hr_k - h^2 & |r_k| > h, \end{cases} \tag{A2}$$

where r_k is the weighted residual of the kth data point and $h = 1.4$, the sum of weighted residuals must first be recast as a sum of uncorrelated weighted residuals. This may be achieved via eigen-decomposition of the covariance matrix:

$$\mathbf{V}_t = \mathbf{Q}\boldsymbol{\Lambda}\mathbf{Q}^T \tag{A3}$$

where $\boldsymbol{\Lambda}$ is the eigenvalue matrix consisting of positive eigenvalues on the diagonals and $\mathbf{Q}$ is the eigenvector matrix. From this we obtain,

$${\mathbf{V}_t}^{-1/2} = \mathbf{Q}\boldsymbol{\Lambda}^{-1/2}\mathbf{Q}^T, \tag{A4}$$

https://doi.org/10.5194/gchron-2022-24
Preprint. Discussion started: 30 September 2022

which can be substituted into equation B1 to give

$$S = \boldsymbol{r}^T \boldsymbol{r}, \tag{A5}$$

where $\boldsymbol{r}$ is a column vector of weighted residuals, given by:

$$\boldsymbol{r} = \mathbf{V}_t{}^{-1/2} (\boldsymbol{t} - \bar{t}\mathbf{1}). \tag{A6}$$

Following the approach in Powell et al., (2020), we minimise $\sum \rho_k$ by finding the $\bar{t}$ value that solves

$$\mathbf{1}^T \mathbf{V}_t{}^{-1/2} \psi(\boldsymbol{r}) = 0, \tag{A7}$$

where,

$$2\psi = \frac{\partial \rho}{\partial r_k}. \tag{A8}$$

This is achieved using an iterative re-weighting procedure, whereby the weight function $w(r_k) = \psi(r_k)/r_k$ is introduced, resulting in

$$\mathbf{1}^T \mathbf{W} \boldsymbol{e} = 0 \tag{A9}$$

with,

$$\boldsymbol{e} = \boldsymbol{t} - \bar{t} \tag{A10}$$

and,

$$\mathbf{W} = \mathbf{W}_h \mathbf{V}_t{}^{-1}, \tag{A11}$$

such that $\mathbf{W}_h$ is a diagonal matrix having $w(r_k)$ as the kkth element. This combines the weighting from w with the weighting from the correlated uncertainties on t. Re-arranging this gives an expression equivalent to equation B13 in Powell et al., (2020),

$$\bar{t} = \mathbf{1}^T \mathbf{W} \boldsymbol{t} \left(\mathbf{1}^T \mathbf{W} \mathbf{1}\right)^{-1} \tag{A12}$$

which can be solved by iteration from a robust starting point (e.g., Maronna, 2019). Analogous to the development of B17 in Powell et al., (2020), uncertainties on $\bar{t}$ are then computed by first-order error propagation as

$$\sigma_t = \frac{1}{\sqrt{\mathbf{1}^T \mathbf{V}_t{}^{-1} \mathbf{I}' \mathbf{1}}} \tag{A13}$$

where $\mathbf{I}' = \mathrm{diag}(\dot{\psi}(\boldsymbol{r}))$.

In the case where all $|r_k| < h$, then $\psi(\boldsymbol{r}) = \boldsymbol{r}$, $\mathbf{W}_h = \mathbf{V}_t{}^{-1}$, and $\mathbf{I}' = \mathbf{I}$, so

$$\bar{t} = \mathbf{1}^T \mathbf{V}_t{}^{-1} \boldsymbol{t} \left(\mathbf{1}^T \mathbf{V}_t{}^{-1} \mathbf{1}\right)^{-1} \tag{A14}$$

and,

$$\sigma_t = \frac{1}{\sqrt{\mathbf{1}^T \mathbf{V}_t{}^{-1} \mathbf{1}}} \tag{A15}$$

yielding the classical statistics result.

https://doi.org/10.5194/gchron-2022-24
Preprint. Discussion started: 30 September 2022

Table B1. Simulated 95 % confidence intervals for $\sqrt{\texttt{mswd}}$ and spine width, s, as a function of the number of data points, n. `DQPB` outputs the one-sided upper 95% confidence limit on s (here denoted *) along with s to assess suitability of the `spine` weighted average algorithm for use with a particular data set.

n	95% CI		$\sqrt{\texttt{mswd}}$	95% CI		s
	Low	High	*	Low	High	*
5	0.348	1.669	1.540	0.12	1.94	1.72
7	0.454	1.552	1.449	0.22	1.83	1.65
9	0.522	1.481	1.392	0.29	1.74	1.59
15	0.634	1.366	1.301	0.43	1.59	1.47
29	0.739	1.260	1.215	0.58	1.42	1.34
59	0.818	1.181	1.151	0.70	1.30	1.24
6	0.408	1.602	1.488	0.21	1.75	1.57
8	0.491	1.513	1.412	0.29	1.70	1.55
10	0.548	1.454	1.371	0.35	1.65	1.52
16	0.646	1.354	1.291	0.46	1.54	1.44
30	0.744	1.256	1.211	0.60	1.41	1.33
60	0.820	1.180	1.149	0.71	1.29	1.24

Appendix B: `spine` weighted average s simulations

To assess whether the central "spine" of data points is sufficiently well-defined to obtain a meaningful weighted average, we compare the spine width, s, to its upper 95% confidence limit bound derived via simulation of Gaussian distributed datasets. Simulations were performed using sample sizes, n, ranging between 5–100 data points. For each n, 10^6 pseudorandom samples were drawn from a standard normal distribution. s values were computed for each sample, and confidence limits on s were estimated based on relevant percentiles (see Table B1). Odd and even n are considered independently in order to account for the effect of small sample biases inherent to `nmad` (e.g., Hayes et al., 2014). The impact of different uncertainty covariance structures on s were also examined, and found to have a negligible effect on these confidence limits.

Appendix C: Robust model 2

The robust data-fitting algorithm in Powell et al. (2020) in the 2-dimensional case, and above, in Appendix A, in the 1-dimensional case, are predicated on the one-sided confidence intervals on the spine width (in Table 1, last column of Powell et al., 2020), and in Table B1 here). The calculation of age, and particularly the uncertainty on age, is appropriate for the case where a dataset gives a spine width that is consistent with the confidence interval.

https://doi.org/10.5194/gchron-2022-24
Preprint. Discussion started: 30 September 2022

Not covered is how best to proceed if in fact a dataset is not consistent with the confidence interval. Whereas the argument developed in Powell et al. (2020), and, by extension here, is that datasets which are consistent are likely to have age significance, this becomes progressively more awkward to argue as the spine width increases. The view taken in this section is that the calculations advocated are for datasets that are considered to have age significance, commonly by geological inference, even though the spine width is outside the confidence interval.

Once the spine width is too large, the data-fitting should plausibly not depend on the analytical uncertainties on the data as these are deemed insufficient to account for the observed scatter. A clear-cut and robust way to proceed is then to discard the analytical uncertainties and rely on the scatter of the data—specifically the spine width—to provide the data uncertainties.

Model 2 in `Isoplot` provides a framework how to proceed. As outlined in the Appendix of Powell et al. (2020), for the `Isoplot` model 2, in which analytical uncertainties are discarded, data are fit y on x, and x on y, and the results combined, circumventing the potentially deleterious effects of error-in-variables effects (e.g., Fuller, 1987). In `Isoplot`, such calculations are done by applying ordinary least squares in the two calculations, giving the slopes, b_{yx} and $1/b_{xy}$, respectively, with the combined slope being given by

$$b = \pm\sqrt{b_{yx}b_{xy}} = \pm\sqrt{\frac{\sum(y_k-\overline{y})^2}{\sum(x_k-\overline{x})^2}} \tag{C1}$$

and,

$$a = \overline{y} - b\overline{x} \tag{C2}$$

(see Powell et al., 2020, for notation and details).

In the equivalent of model 2 using the `spine` algorithm, the analytical uncertainties are discarded, then the spine width is calculated from the scatter of the data about the line, $s = \mathtt{nmad}(e)$. The development in Appendix B of Powell et al. (2020) can be applied as-is to the two calculations required: y on x, and x on y, except that two definitions need to be changed: eq B5[1] should involve $\mathbf{W}_e$ with diagonal elements, $1/s$, and eq B13 should involve $\mathbf{W}$ with diagonal elements, $w(r_k)/s^2$.

Applying spline algorithm in the above-modified form to fitting y on x, and x on y, allows the slope, $b = \pm\sqrt{b_{yx}b_{xy}}$ to be calculated, and the intercept a, as in (ref. eq. in Powell 2020). The covariance matrix for each slope plus intercept can be calculated by eq B17. Combination into a covariance matrix for $\{a, b\}$ requires the observation that b_{yx} and b_{xy} are uncorrelated. An error propagation is then straightforward to b, and in fact a good approximation is generally given by adding the constituent covariance matrices and dividing by 4.

Code availability. The `BQPB` source code and compiled versions of of the GUI application may be obtained from the repositories described in Sect. 9.

[1] the equation numbers here refer to those in Powell et al. (2020)

https://doi.org/10.5194/gchron-2022-24
Preprint. Discussion started: 30 September 2022

Author contributions. JW and JH devised the initial concept with input from JE and TP. TP devised the computational approaches and wrote the software with assistance from JE and JH. RP and TP devised the spine weighted average approach. RP devised the robust model 2 approach and wrote the code for it. TP prepared the manuscript with contributions from all co-authors.

Competing interests. The authors declare that they have no conflict of interest.

Acknowledgements. Shuhei Sakata kindly provided the unpublished Sambe-Kisuki zircon data. This research was supported by Australian Research Council grants DP110102185 (to RD, JW and JH), DP160102969 (to RD and JW) and FL160100028 (to JW).

https://doi.org/10.5194/gchron-2022-24
Preprint. Discussion started: 30 September 2022

References

Albarède, F.: Introduction to Geochemical Modeling, Cambridge University Press, Cambridge, https://doi.org/10.1017/CBO9780511622960, 1995.

Bajo, P., Drysdale, R., Woodhead, J., Hellstrom, J., and Zanchetta, G.: High-Resolution u-Pb Dating of an Early Pleistocene Stalagmite from Corchia Cave (Central Italy), Quaternary Geochronology, 14, 5–17, https://doi.org/10.1016/j.quageo.2012.10.005, 2012.

Bateman, H.: Solution of a System of Differential Equations Occurring in the Theory of Radioactive Transformations: Proceedings of the Cambridge Philosophical Society, Proceedings of the Cambridge Philosophical Society, 15, 423–427, 1910.

Chew, D. M., Sylvester, P. J., and Tubrett, M. N.: U–Pb and Th–Pb Dating of Apatite by LA-ICPMS, Chemical Geology, 280, 200–216, https://doi.org/10.1016/j.chemgeo.2010.11.010, 2011.

Crowley, J. L., Schoene, B., Bowring, S. A.: U-Pb dating of zircon in the Bishop Tuff at the millennial scale, Geology, 35, 1123–1126, https://doi.org/https://doi.org/10.1130/G24017A.1, 2007.

Drysdale, R. N., Paul, B. T., Hellstrom, J. C., Couchoud, I., Greig, A., Bajo, P., Zanchetta, G., Isola, I., Spötl, C., Baneschi, I., Regattieri, E., and Woodhead, J. D.: Precise Microsampling of Poorly Laminated Speleothems for U-series Dating, Quaternary Geochronology, 14, 38–47, https://doi.org/10.1016/j.quageo.2012.06.009, 2012.

Engel, J. and Pickering, R.: The Role of Inherited Pb in Controlling the Quality of Speleothem U-Pb Ages, Quaternary Geochronology, 67, 101 243, https://doi.org/10.1016/j.quageo.2021.101243, 2022.

Engel, J., Woodhead, J., Hellstrom, J., Maas, R., Drysdale, R., and Ford, D.: Corrections for Initial Isotopic Disequilibrium in the Speleothem U-Pb Dating Method, Quaternary Geochronology, 54, 101 009, https://doi.org/10.1016/j.quageo.2019.101009, 2019.

Engel, J., Maas, R., Woodhead, J., Tympel, J., and Greig, A.: A Single-Column Extraction Chemistry for Isotope Dilution U-Pb Dating of Carbonate, Chemical Geology, 531, 119 311, https://doi.org/10.1016/j.chemgeo.2019.119311, 2020.

Fuller, W. R.: Measurement error models, John Wiley and Sons, 440 pp., 1987.

Getty, S. R. and DePaolo, D. J.: Quaternary Geochronology Using the U-Th-Pb Method, Geochimica et Cosmochimica Acta, 59, 3267–3272, https://doi.org/10.1016/0016-7037(95)00197-8, 1995.

Getty, S. R., Asmerom, Y., Quinn, T. M., and Budd, A. F.: Accelerated Pleistocene Coral Extinctions in the Caribbean Basin Shown by Uranium-Lead (U-Pb) Dating, Geology, 29, 639–642, https://doi.org/10.1130/0091-7613(2001)029<0639:APCEIT>2.0.CO;2, 2001.

Guillong, M., von Quadt, A., Sakata, S., Peytcheva, I., and Bachmann, O.: LA-ICP-MS Pb-U Dating of Young Zircons from the Kos–Nisyros Volcanic Centre, SE Aegean Arc, Journal of Analytical Atomic Spectrometry, 29, 963–970, https://doi.org/10.1039/C4JA00009A, 2014.

Harris, C. R., Millman, K. J., van der Walt, S. J., Gommers, R., Virtanen, P., Cournapeau, D., Wieser, E., Taylor, J., Berg, S., Smith, N. J., et al.: Array Programming with NumPy, Nature, 585, 357–362, 2020.

Hayes, K.: Finite-Sample Bias-Correction Factors for the Median Absolute Deviation, Communications in Statistics–simulation and computation, 43, 2205–2212, https://doi.org/10.1080/03610918.2012.748913, 2014.

Hattori, K., Sakata, S., Tanaka, M., Orihashi, Y., and Hirata, T.: U–Pb Age Determination for Zircons Using Laser Ablation-ICP-mass Spectrometry Equipped with Six Multiple-Ion Counting Detectors, Journal of Analytical Atomic Spectrometry, 32, 88–95, https://doi.org/10.1039/C6JA00311G, 2017.

Hellstrom, J. C.: Rapid and Accurate U/Th Dating Using Parallel Ion-Counting Multi-Collector ICP-MS, Journal of Analytical Atomic Spectrometry, 18, 1346, https://doi.org/10.1039/b308781f, 2003.

https://doi.org/10.5194/gchron-2022-24
Preprint. Discussion started: 30 September 2022

Hunter, J. D.: Matplotlib: A 2D graphics environment, Computing in Science & Engineering, 9, 90–95, https://doi.org/10.1109/MCSE.2007.55, 2007.

Ickert, R. B., Mundil, R., Magee, C. W., and Mulcahy, S. R.: The U–Th–Pb Systematics of Zircon from the Bishop Tuff: A Case Study in Challenges to High-Precision Pb/U Geochronology at the Millennial Scale, Geochimica et Cosmochimica Acta, 168, 88–110, https://doi.org/10.1016/j.gca.2015.07.018, 2015.

Ito, H., Nanayama, F., and Nakazato, H.: Zircon U–Pb dating using LA-ICP-MS: Quaternary tephras in Boso Peninsula, Japan, Quaternary Geochronology, 40, 12–22, https://doi.org/10.1016/j.quageo.2016.07.002, 2017.

Ivanovich, M. and Harmon, R. S.: Uranium-Series Disequilibrium: Applications to Earth, Marine, and Environmental Sciences., Clarendon Press, United Kingdom, second edn., 1992.

Ludwig, K. R.: Effect of Initial Radioactive-Daughter Disequilibrium on U-Pb Isotope Apparent Ages of Young Minerals, Journal of Research of the US Geological Survey, 5, 663–667, 1977.

Ludwig, K. R.: On the Treatment of Concordant Uranium-Lead Ages, Geochimica et Cosmochimica Acta, 62, 665–676, https://doi.org/10.1016/S0016-7037(98)00059-3, 1998.

Ludwig, K. R.: Mathematical–Statistical Treatment of Data and Errors for ^{230}Th/U Geochronology, in: Reviews in Mineralogy & Geochemistry, pubs.geoscienceworld.org, 2003.

Ludwig, K. R.: Isoplot/Ex Version 3.75: A Geochronological Toolkit for Microsoft Excel, Special Publication 4, Berkeley Geochronology Center, 2012.

Maronna, R. A., Martin, D., Yohai, V. J., Salibián-Barrera, M. Robust statistics. John Wiley and Sons, Chichester, 2019.

Mattinson, J. M.: Anomalous Isotopic Composition of Lead in Young Zircons, in: Carnegie Institution Washington Yearbook 72, pp. 613–616, 1973.

McLean, N. M., Bowring, J. F., and Bowring, S. A.: An Algorithm for U-Pb Isotope Dilution Data Reduction and Uncertainty Propagation, Geochemistry, Geophysics, Geosystems, 12, https://doi.org/10.1029/2010GC003478, 2011.

Neymark, L. A., Amelin, Y. V., and Paces, J. B.: ^{206}Pb-^{230}Th-^{234}U-^{238}U and ^{207}Pb-^{235}U Geochronology of Quaternary Opal, Yucca Mountain, Nevada, Geochimica et Cosmochimica Acta, 64, 2913–2928, https://doi.org/10.1016/S0016-7037(00)00408-7, 2000.

Oliphant, T. E.: Python for scientific computing, Computing in science & engineering, 9, 10–20, https://doi.org/10.1109/MCSE.2007.58, 2007.

Osmond, J. K. and Cowart, J. B.: Groundwater, in: Uranium-Series Disequilibrium and Applications to Environmental Problems, Oxford Science Publications, Oxford, second edn., 1992.

Paquette, J.-L., Médard, E., Francomme, J., Bachèlery, P., and Hénot, J.-M.: LA-ICP-MS U/Pb Zircon Timescale Constraints of the Pleistocene Latest Magmatic Activity in the Sancy Stratovolcano (French Massif Central), Journal of Volcanology and Geothermal Research, 374, 52–61, https://doi.org/10.1016/j.jvolgeores.2019.02.015, 2019.

Pickering, R., Dirks, P. H. G. M., Jinnah, Z., de Ruiter, D. J., Churchill, S. E., Herries, A. I. R., Woodhead, J. D., Hellstrom, J. C., and Berger, L. R.: Australopithecus Sediba at 1.977 Ma and Implications for the Origins of the Genus Homo, Science, 333, 1421–1423, https://doi.org/10.1126/science.1203697, 2011.

Powell, R. and Holland, T.: An Internally Consistent Dataset with Uncertainties and Correlations: 3. Applications to Geobarometry, Worked Examples and a Computer Program, Journal of Metamorphic Geology, 6, 173–204, https://doi.org/10.1111/j.1525-1314.1988.tb00415.x, 1988.

https://doi.org/10.5194/gchron-2022-24
Preprint. Discussion started: 30 September 2022

Powell, R., Hergt, J., and Woodhead, J.: Improving Isochron Calculations with Robust Statistics and the Bootstrap, Chemical Geology, pp. 191–204, 2002.

Powell, R., Green, E. C. R., Marillo Sialer, E., and Woodhead, J.: Robust Isochron Calculation, Geochronology, 2, 325–342, https://doi.org/10.5194/gchron-2-325-2020, 2020.

Rasbury, E. T. and Cole, J. M.: Directly Dating Geologic Events: U-Pb Dating of Carbonates, Reviews of Geophysics, 47, 261–27, https://doi.org/10.1029/2007RG000246, 2009.

Richards, D. A., Bottrell, S. H., Cliff, R. A., Ströhle, K., and Rowe, P. J.: U-Pb Dating of a Speleothem of Quaternary Age, Geochimica et Cosmochimica Acta, 62, 3683–3688, https://doi.org/10.1016/S0016-7037(98)00256-7, 1998.

Rioux, M., Johan Lissenberg, C., McLean, N. M., Bowring, S. A., MacLeod, C. J., Hellebrand, E., and Shimizu, N.: Protracted Timescales of Lower Crustal Growth at the Fast-Spreading East Pacific Rise, Nature Geoscience, 5, 275–278, https://doi.org/10.1038/ngeo1378, 2012.

Rock, N. and Duffy, T.: REGRES: A FORTRAN-77 Program to Calculate Nonparametric and "Structural" Parametric Solutions to Bivariate Regression Equations, Computers & Geosciences, 1986.

Rock, N., Webb, J., McNaughton, N., and Bell, G.: Nonparametric Estimation of Averages and Errors for Small Data-Sets in Isotope Geoscience: A Proposal, Chemical Geology: Isotope Geoscience section, 66, 163–177, https://doi.org/10.1016/0168-9622(87)90038-8, 1987.

Sakata, S.: A Practical Method for Calculating the U-Pb Age of Quaternary Zircon: Correction for Common Pb and Initial Disequilibria, Geochemical Journal, 52, 281–286, https://doi.org/10.2343/geochemj.2.0508, 2018.

Sakata, S., Hattori, K., and and, H. I. G.: Determination of U–Pb Ages for Young Zircons Using Laser Ablation-ICP-mass Spectrometry Coupled with an Ion Detection Attenuator Device, Wiley Online Library, https://doi.org/10.1111/j.1751-908X.2014.00320.x, 2014.

Sakata, S., Hirakawa, S., Iwano, H., Danhara, T., Guillong, M., and Hirata, T.: A New Approach for Constraining the Magnitude of Initial Disequilibrium in Quaternary Zircons by Coupled Uranium and Thorium Decay Series Dating, Quaternary Geochronology, 38, 1–12, https://doi.org/10.1016/j.quageo.2016.11.002, 2017.

Schoene, B.: U–Th–Pb Geochronology, in: Treatise on Geochemistry 2nd Edition, pp. 341–378, Elsevier, 2014.

Schärer, U.: The Effect of Initial ^{230}Th Disequilibrium on Young U-Pb Ages: The Makalu Case, Himalaya, Earth and Planetary Science Letters, 67, 191–204, 1984.

Stacey, J. S. and Kramers, J. D.: Approximation of Terrestrial Lead Isotope Evolution by a Two-Stage Model, Earth and Planetary Science Letters, 26, 207–221, https://doi.org/10.1016/0012-821X(75)90088-6, 1975.

Tera, F. and Wasserburg, G. J.: U-Th-Pb Systematics in Lunar Highland Samples from the Luna 20 and Apollo 16 Missions, Earth and Planetary Science Letters, 17, 36–51, https://doi.org/10.1016/0012-821X(72)90257-9, 1972.

Titterington, D. M. and Halliday, A. N.: On the Fitting of Parallel Isochrons and the Method of Maximum Likelihood, Chemical Geology, 26, 183–195, 1979.

Vermeesch, P.: IsoplotR: A Free and Open Toolbox for Geochronology, Geoscience Frontiers, 9, 1479–1493, https://doi.org/10.1016/j.gsf.2018.04.001, 2018.

Virtanen, P., Gommers, R., Oliphant, T. E., Haberland, M., Reddy, T., Cournapeau, D., Burovski, E., Peterson, P., Weckesser, W., Bright, J., van der Walt, S. J., Brett, M., Wilson, J., Millman, K. J., Mayorov, N., Nelson, A. R. J., Jones, E., Kern, R., Larson, E., Carey, C. J., Polat, I., Feng, Y., Moore, E. W., VanderPlas, J., Laxalde, D., Perktold, J., Cimrman, R., Henriksen, I., Quintero, E. A., Harris, C. R., Archibald, A. M., Ribeiro, A. H., Pedregosa, F., van Mulbregt, P., and SciPy 1.0 Contributors: SciPy 1.0: Fundamental Algorithms for Scientific Computing in Python, Nature Methods, 17, 261–272, https://doi.org/10.1038/s41592-019-0686-2, 2020.

https://doi.org/10.5194/gchron-2022-24
Preprint. Discussion started: 30 September 2022

von Quadt, A., Gallhofer, D., Guillong, M., Peytcheva, I., Waelle, M., and Sakata, S.: U–Pb Dating of CA/Non-CA Treated Zircons Obtained by LA-ICP-MS and CA-TIMS Techniques: Impact for Their Geological Interpretation, Journal of Analytical Atomic Spectrometry, 29, 1618–1629, https://doi.org/10.1039/C4JA00102H, 2014.

Wendt, I. and Carl, C.: U/Pb Dating of Discordant 0.1 Ma Old Secondary U Minerals, Earth and Planetary Science Letters, 73, 278–284, 1985.

Wendt, I. and Carl, C.: The Statistical Distribution of the Mean Squared Weighted Deviation, Chemical Geology: Isotope Geoscience section, 86, 275–285, https://doi.org/10.1016/0168-9622(91)90010-T, 1991.

Woodhead, J. and Pickering, R.: Beyond 500ka: Progress and Prospects in the U-Pb Chronology of Speleothems, and Their Application to Studies in Palaeoclimate, Human Evolution, Biodiversity and Tectonics, Chemical Geology, 322–323, 290–299, https://doi.org/10.1016/j.chemgeo.2012.06.017, 2012.

Woodhead, J., Hellstrom, J., Pickering, R., Drysdale, R., Paul, B., Bajo, P.,: U and Pb variability in older speleothems and strategies for their chronology , Quaternary Geochronology, 14, 105–113, https://doi.org/10.1016/j.quageo.2012.02.028, 2012.

Woodhead, J., Hellstrom, J., Maas, R., Drysdale, R., Zanchetta, G., Devine, P., and Taylor, E.: U–Pb Geochronology of Speleothems by MC-ICPMS, Quaternary Geochronology, 1, 208–221, https://doi.org/10.1016/j.quageo.2006.08.002, 2006.

York, D.: Least-Squares Fitting of a Straight Line, Canadian Journal of Physics, 44, 1–8, 1969.

York, D., Evensen, N. M., Martı´nez, M. L., and De Basabe Delgado, J.: Unified Equations for the Slope, Intercept, and Standard Errors of the Best Straight Line, American Journal of Physics, 72, 367–375, https://doi.org/10.1119/1.1632486, 2004.